Acta Crystallographica Section D
Biological Crystallography
ISSN 0907-4449

X-ray scattering studies of *Aspergillus flavus* urate oxidase: towards a better understanding of PEG effects on the crystallization of large proteins

D. Vivarès and F. Bonneté*

Laboratoire de Minéralogie Cristallographie, UMR 7590 CNRS, Universités Paris 6–Paris 7–IPG, Case 115, 4 Place Jussieu, F-75252 Paris CEDEX 05, France

Correspondence e-mail: bonnete@lmcp.jussieu.fr

Received 14 September 2001
Accepted 2 January 2002

The determination of the three-dimensional structures of biological macromolecules by X-ray diffraction generally requires large good-quality crystals, which are often difficult to obtain as crystal nucleation and growth depend upon a great number of physicochemical parameters. In the future, the emergence of structural genomic projects will require new and rapid methods to determine crystallization conditions. Until now, the prediction of crystallization conditions has essentially been based on the knowledge of interparticular interactions in solutions inferred from studies on small soluble proteins in the presence of salts. The present study, by small-angle X-ray scattering, of urate oxidase from *Aspergillus flavus*, a homotetrameric enzyme of 128 kDa, allowed the extension of the results to the crystallization of large proteins in the presence of polyethylene glycol (PEG). The protein crystallization, the nucleation rate and the different morphological crystal shapes obtained were correlated with the second virial coefficient (A_2), which was found to be in a restricted range at the low end of the 'crystallization slot' proposed by George & Wilson [(1994). *Acta Cryst.* D**50**, 361–365].

1. Introduction

In the field of structural biology, the main technique for the determination of the three-dimensional structures of macromolecules (proteins, nucleic acids, macromolecular complexes, viruses *etc.*) remains crystallography – more than 80% of structures are solved by the diffraction of X-rays. In addition, with the constant improvement in X-ray sources, in data-collection instruments and in data analysis, the number of known structures has increased tremendously over past decades. Paradoxically, it is crystallization, still too often governed by trial-and-error methods, that remains the limiting stage of crystallography. Better understanding of the factors that control the nucleation and crystal growth of macromolecules is of prime importance, especially in the context of genome sequencing.

It is now admitted that phase transitions such as liquid–liquid or liquid–solid (crystal or precipitate) phase separations are governed by weak interaction forces between macromolecules in solution: hard-sphere forces, coulombic repulsions, van der Waals attractions *etc.* Studies have notably been performed on different model systems to find a way to correlate the interactions of macromolecules in solution with crystallization. Various parameters (pH, temperature, addition of crystallizing agent) were systematically and independently studied. Such studies are intended to develop more rational approaches that could help crystallographers to limit crystallization conditions.

The first and most studied protein molecule is lysozyme, which crystallizes easily on the addition of salts (sodium thiocyanate, sodium chloride *etc.*). In this case, it was shown by small-angle X-ray and static light scattering that the global interactions between particles were modified from repulsive to attractive by the addition of salt, leading to the crystallization process (Muschol & Rosenberger, 1995; Ducruix *et al.*, 1996). In addition, a differential anion effect was observed with lysozyme and various other systems, which affects both solubility (Riès-Kautt & Ducruix, 1989; Carbonnaux *et al.*, 1995; Veesler *et al.*, 1996) and macromolecular interactions whatever the size, the isoelectric point and the compactness of the protein (Ducruix *et al.*, 1996; Lafont *et al.*, 1997; Bonneté *et al.*, 1999, 2001; Budayova *et al.*, 1999; Finet, 1999; Tardieu *et al.*, 1999; Piazza & Pierno, 2000). This differential effect follows the direct or reverse order of the Hofmeister series (Hofmeister, 1888), depending on whether the pH of the solution is above or below the isoelectric point of the protein, respectively.

A thermodynamic parameter, the second virial coefficient A_2 (often written B_{22} in static light-scattering experiments) was found to be suitable to characterize the net intermolecular forces in solution, as it is negative with net attractive protein–protein interactions and positive with repulsive ones. George & Wilson (1994) have shown by compiling the data from a diverse set of soluble proteins crystallized with various precipitant agents that the soluble proteins crystallize in a narrow range of the second virial coefficient (about -1.0 to -8.0×10^{-4} mol ml g^{-2}) which they called the 'crystallization slot', corresponding to slight attractive interactions between particles. The second virial coefficient therefore appeared to be a useful tool to predict the crystallization of proteins. This observation was later confirmed in the case of addition of salt to different proteins such as lysozyme (Bonneté *et al.*, 1999; Guo *et al.*, 1999; Haas *et al.*, 1999), BPTI (Lafont *et al.*, 1997), chymotrypsinogen (Velev *et al.*, 1998) or apoferritin (Petsev *et al.*, 2000). Although some interaction studies between macromolecules have been performed with the widely used non-adsorbing polymer PEG (polyethylene glycol; Budayova *et al.*, 1999; Kulkarni *et al.*, 2000; Finet & Tardieu, 2001), only a few works correlate the second virial coefficient with protein crystallization (Hitscherich *et al.*, 2000).

In previous work, we used urate oxidase from *A. flavus* as a new model system for crystallogenesis. Its three-dimensional structure in complex with the inhibitor 8-azaxanthine was solved at 2.05 Å resolution (Colloc'h *et al.*, 1997). The active enzyme is a homotetrameric globular protein (monomeric subunit of about 32 kDa) with an external diameter of 70 Å, enclosing a tunnel 70 Å long and 15 Å in diameter. It is composed of two homodimers superimposed head-to-tail, each dimer being composed of two monomers related by a crystallographic twofold axis.

Its interactions in solution were characterized by small-angle X-ray scattering under conditions where the enzyme is most active and stable (Bonneté *et al.*, 2001). Under these conditions, urate oxidase presented slightly repulsive interactions. Changing the pH or adding salt (300 m*M* sodium thiocyanate and 1 *M* sodium formate) was found to be ineffective to induce attractive interactions and protein crystallization. Experiments performed with the addition of PEG first showed a correlation between crystallization and attractive interactions of urate oxidase in solution, which suggested that this protein could be an excellent system for crystallogenesis studies.

In the present work, the interactions of urate oxidase in solution were first studied by SAXS as a function of addition of other salts close to the pI (at pH 8.5) and far from the pI (at pH 10.5). Our studies were limited to medium salt concentrations (up to 500 m*M*); it is noteworthy that at high salt concentrations a variety of effects which are not fully understood can occur (Boyer *et al.*, 1999; Ebel *et al.*, 1999; Petsev *et al.*, 2000). Furthermore, as the addition of PEG was found to be more effective close to the isoelectric point (Bonneté *et al.*, 2001), the effects of PEGs of different molecular weights (3350, 8000 and 20 000 Da) and at various concentrations were studied mainly at pH 8.5.

Whatever the pH of the solution, the addition of salts was found to be ineffective to induce attractive interactions, in contrast to the case with small soluble proteins (lysozyme, BPTI or γ-crystallins); this result is discussed by coupling SAXS experiments with numerical simulations based on a simple model from colloid physics, the DLVO (Derjaguin–Landau–Verwey–Overbeek) model (Derjaguin & Landau, 1941; Verwey & Overbeek, 1948). On the other hand, PEG is shown to induce an attractive interaction between proteins which increases with both the size and the concentration of polymer.

In parallel with the SAXS experiments, crystallization trials were performed and attractive interactions observed by addition of PEG could be correlated with the crystallization of urate oxidase. Nucleation and crystal shapes were found to change with the weight and the concentration of the polymer, as did the second virial coefficient. In addition, our results indicate that the crystallization of urate oxidase occurs in a restricted range of the second virial coefficient at the low end of the 'crystallization slot' defined by George and Wilson (1994).

2. Materials and methods

2.1. Preparation of urate oxidase

Urate oxidase solution was prepared as described previously (Bonneté *et al.*, 2001). Several protein solutions were then prepared in buffers at different pH values (50 m*M* Tris pH 7.5, 8.0, 8.5, 9.1, 50 m*M* sodium borate pH 8.7 and 10 m*M* sodium carbonate pH 10.5) by diluting the stock solution with the appropriate pH buffer and concentrating this new solution in an Amicon cell. This process was repeated several times to ensure that the protein solution was at the desired pH. All solutions were finally adjusted to a concentration of about 60 mg ml^{-1}.

2.2. Preparation of PEG and salt solutions

All PEG (from Hampton Research) and salt (from Sigma) solutions for the SAXS experiments and the crystallization trials were buffered at a given pH with appropriate buffers. All solutions were filtered through 0.22 µm Millipore filters. The stock solutions 2 *M* sodium acetate and sodium sulfate, 40% PEG 3350, 40% PEG 8000 and 20% PEG 20 000 were prepared and buffered at the appropriate pH. Concentrations of PEG solutions are expressed in weight per volume.

2.3. Crystallization trials

The crystallization trials were performed in an air-conditioned room (293 K) with the microbatch technique. Droplets were prepared by mixing 2 µl of a concentrated and purified protein solution with 2 µl of precipitant agent and pipetted under a layer of paraffin oil in a 72-well microbatch plate (paraffin oil and plates from Hampton Research). Crystals were observed with a TE 200 microscope from Nikon and photographs were taken with the software *Replay* developed by Microvision, with an enlargement of 200.

2.4. Solution X-ray scattering measurements

X-ray scattering curves were recorded with the small-angle scattering instrument D24 using the synchrotron radiation emitted by the storage ring DCI at LURE (Orsay). The instrument, the data-acquisition system and the thermostatted cell under vacuum used for these experiments have been described previously (Boulin *et al.*, 1986; Depautex *et al.*, 1987; Dubuisson *et al.*, 1997). The wavelength of the X-rays was 1.488 Å (Ni *K* edge). The sample-to-detector distances used in the different series of experiments were 1890 $\pm$ 5 mm, yielding an s increment per channel of $2.15 \pm 0.005 \times 10^{-4}$ A^{-1}. One to six frames with duration of 200 s each according to the protein concentration were recorded for each sample and corresponding buffers. The curves were scaled to the transmitted intensity. After subtraction of the appropriate buffer, the curves were normalized to the enzyme concentration before plotting.

3. Theory

3.1. Interaction forces

Proteins in solution interact through non-specific medium-range (from a few angstroms to a few tens of angstroms) interaction forces. Three interactions are well identified: the repulsive hard-sphere interaction, which characterizes the fact that proteins cannot interpenetrate, the repulsive coulombic interaction arising from the net charge of the protein and the attractive van der Waals component, which is the resulting dipolar interaction between proteins. These three interactions, which depend on pH, temperature and solvent composition, constitute what is called the DLVO model.

Proteins in solution also interact through other non-specific forces such as hydration or hydrophobic forces, which are still poorly characterized. The addition of precipitating agents (salts or PEG) can also induce other additional attractive forces. The attractive interaction induced by the addition of polymer is the depletion attraction, which is a function of the polymer mass and concentration (Lekkerkerker, 1997; Kulkarni *et al.*, 2000; Vliegenthart & Lekkerkerker, 2000). This depletion interaction, which was originally described in the case of colloid–polymer mixtures (Asakura & Oosawa, 1954; Vrij, 1976) and subsequently in the case of protein–polymer mixtures (Mahadevan & Hall, 1990) can be explained in a simplified manner (Fig. 1) for an ideal polymer solution. Molecules of polymer (characterized by their radius of gyration R_g) and colloids cannot mutually interpenetrate; furthermore, the centre of polymers is excluded from a region of thickness R_g around each colloidal particle. This region is called the depletion zone. When two colloid particles come sufficiently close to each other, their depletion zones overlap and the free volume accessible to the polymer molecules increases, leading to a gain in entropy of the system. Thermodynamically, it is therefore more favourable for the polymer that the colloidal particles become closer, which corresponds to an attractive interaction between them. This model remains valid as long as molecules of polymer do not overlap.

3.2. Small-angle X-ray scattering

The second virial coefficient A_2, which characterizes the resultant force of all individual interactions, is determined in this case by small-angle X-ray scattering (SAXS). The total normalized intensity $I(c, s)$ scattered by a solution of monodisperse spherical particles at a scattering angle 2θ can be expressed as a function of the particle concentration c and the modulus of the scattering vector **s**, $s = 2\lambda^{-1}\sin\theta$, by

$$I(c,s) = I(0,s)S(c,s). \tag{1}$$

$I(0, s)$, the intensity scattered by one particle and usually called the particle form factor, is the Fourier transform of the spherically averaged auto-correlation function of the electron-density contrast associated with the particle. The form factor is generally obtained from curves recorded at low concentrations to avoid interaction effects.

With interacting spherical particles, departure from ideality may simply be accounted for by a multiplying factor or interference term, $S(c, s)$, usually called the solution structure factor. The nature of the net interactions, either attractive or repulsive, can be simply determined by the plot of the struc-

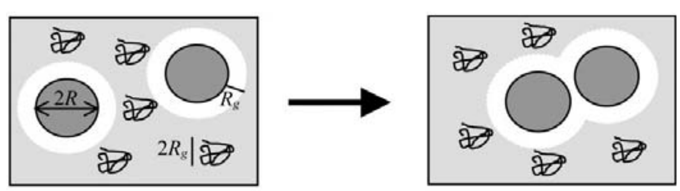

Figure 1
The depletion zone around each protein molecule where the centres of polymer molecules cannot enter is in white. When the depletion zones overlap, the volume accessible to the polymer increases, giving rise to an entropy-driven depletion attraction between proteins.

ture factor at the origin, $S(c, 0)$, as a function of the particle concentration, since it is related to the osmotic pressure Π by

$$S(c,0) = \frac{RT}{M}\left(\frac{\partial \Pi}{\partial c}\right)^{-1}, \tag{2}$$

with

$$\frac{\Pi}{cRT} = \frac{1}{M} + A_2 c + A_3 c^2 + \ldots, \tag{3}$$

the concentration c being expressed in g cm^{-3}.

Therefore, the second virial coefficient can be obtained by the expression

$$S(c,0) = \frac{I(c,0)}{I(0,0)} = \frac{1}{1 + 2MA_2c + \ldots}. \tag{4}$$

In the case where the term $2MA_2c$ is small (<<1), the expansion in powers of c of the structure factor at the origin $S(c, 0)$ can be limited to the second virial coefficient and linearized. Experimentally, the structure factor at the origin is evaluated from the expression

$$S(c,0) = \frac{\lim_{s\to 0} I(c,s)}{\lim_{c\to 0} I(c,0)}. \tag{5}$$

The slope of the linear fit gives the coefficient A_2 in mol ml g^{-2},

$$\frac{1}{S(c,0)} = 1 + 2MA_2c. \tag{6}$$

If A_2 is positive, the overall interactions are repulsive; if A_2 is negative, the interactions are attractive.

4. Results

4.1. Temperature effects

In previous work (Bonneté *et al.*, 2001), a slight temperature effect was observed on the scattered intensity at small angles at pH 10.5 between 283 and 293 K, which was attributed to a small van der Waals attraction. In order to characterize it in terms of second virial coefficient, SAXS experiments were performed over a larger range of temperature from 278 to 303 K at a constant pH closer to the isoelectric point, where the repulsive component is weaker. Since the Tris buffer was very sensitive to variations of temperature ($dpK_a/dT = -0.028$; Beynon & Easterby, 1996), we used a 50 m*M* sodium borate buffer whose pH is known to be less temperature dependent ($dpK_a/dT = -0.008$). Values of the second virial coefficient were determined from SAXS experiments as a function of urate oxidase concentration at each temperature (Table 1). The second virial coefficient, while sharply increasing with the temperature, remains positive.

It is worth noting that at 277 K some crystals grew after several weeks in the absence of any crystallizing agent whatever the pH of the solution (pH 8.5–10.5; data not shown). The crystallographic structure was determined from crystals grown in 10 m*M* sodium carbonate pH 10.5 at 277 K (Colloc'h *et al.*, 1997). According to Table 1, this shows that urate oxidase can crystallize with a second virial coefficient A_2 close to zero.

Table 1
Variations of second virial coefficient as a function of temperature in 50 m*M* sodium borate pH 8.7.

T (K)	A_2 ($10^{-4} \pm 5 \times 10^{-6}$ mol ml g^{-2})
278	+0.09
283	+0.17
293	+0.24
303	+0.36

4.2. pH and salt effects: SAXS experiments

Small-angle X-ray scattering experiments were performed with solutions of urate oxidase at different concentrations in the presence of its inhibitor at pH 8.5 and 10.5. A compilation of second virial coefficient (A_2) values of urate oxidase determined from these SAXS experiments and from a previous work (Bonneté *et al.*, 2001) are plotted in Fig. 2 as a function of pH between pH 7.5 and 10.5. Below pH 7.5 and above pH 10.5, the protein is unstable (Bayol *et al.*, 1995). A_2 is minimum between pH 7.5 and 8.0 and then sharply increases until pH 10.5. This result was expected, as the theoretical isoelectric point is about 7.7. Consequently, by changing the pH away from the pI (pH > 8.0) the protein net charge increases, leading to an increase in the repulsive electrostatic interactions.

Experiments were performed with addition of salts at two pH values close (pH 8.5) and far (pH 10.5) from the isoelectric point (pI) of the protein. With model systems such as lysozyme, the protein interactions in solution weakly depend on the nature of the cation and are strongly dependent on the kind of anion (Ducruix *et al.*, 1996). We therefore focused our study on the anion effect using sodium salts. As the pH values

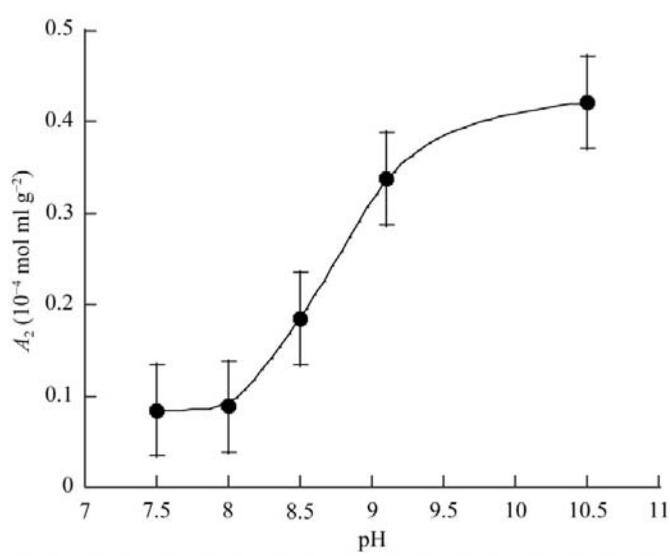

Figure 2
Variations of the second virial coefficient as a function of the pH of urate oxidase solutions with error bars of $\pm 5 \times 10^{-6}$ mol ml g^{-2} (the line is drawn as a guide).

of the solutions studied were above the isoelectric point (pH 8.5 and pH 10.5), the monovalent and divalent sodium salts chosen from the Hofmeister series which were *a priori* the most efficient for inducing attractive interactions and protein crystallization (Carbonnaux *et al.*, 1995; Veesler *et al.*, 1996) were sodium acetate and sodium sulfate.

Values of the second virial coefficient at pH 8.5 and 10.5 without salt and with sodium acetate or sulfate are summarized in Table 2. At pH 8.5 or 10.5, adding salts to any concentration up to 500 m*M* did not bring the solution into an attractive regime. The values of the second virial coefficient measured in 100 and 500 m*M* sodium acetate and 400 m*M* sodium sulfate at pH 8.5 and in 500 m*M* sodium acetate at pH 10.5 are about the same as those at pH 7.5 or 8.0, values close to the pI. At pH 10.5, the effect of salt addition is progressive until the screening of the charges on the surface of the molecule. At pH 8.5, the values at 100 and 500 m*M* are close to each other and inverted, but are not different enough to be attributable to an increase of the repulsion as observed with apoferritin (Petsev & Vekilov, 2000). In a previous study, charge screening was also observed at pH 9.1 with two other salts, sodium formate and sodium thiocyanate (Bonneté *et al.*, 2001). All these studies confirm that in the case of urate oxidase the only role of salts seems to be the screening of electrostatic repulsion.

Crystallization trials were performed under identical conditions in an air-conditioned room at about 293 K. No crystal were obtained after several weeks.

Table 2
Values of the second virial coefficient with and without salt added in Tris buffer at pH 8.5 and in sodium carbonate pH 10.5 at 293 K.

	A_2 ($10^{-4} \pm 5 \times 10^{-6}$ mol ml g^{-2})			
pH	Without salt	100 m*M* sodium acetate	500 m*M* sodium acetate	400 m*M* sodium sulfate
8.5	+0.19	+0.09	+0.11	+0.14
10.5	+0.42	+0.24	+0.14	

4.3. pH and salt effects: numerical simulations

The pH and salt effects observed on the variations of the second virial coefficient can be simply explained by a decrease in the coulombic repulsive interactions, owing to the decrease of the protein net charge by either changing the pH close to the pI or by screening the repulsion with salt. This assumption was checked by characterizing not only the global interactions between proteins, expressed by A_2, but also each of the different underlying interaction potentials. For this purpose, numerical simulations were performed on series of SAXS experiments on urate oxidase at different pH values without salt and at pH 8.5 and 10.5 with addition of 100 and 500 m*M* sodium acetate.

Details of the theoretical treatment have been described elsewhere (Malfois *et al.*, 1996; Tardieu *et al.*, 1999). We used an iterative program developed by Luc Belloni (Belloni, 1991) with a simplified model that takes into account the protein–protein interactions. The macromolecular particles are considered as spheres of net charge Z and the ions are treated as points and appear only through the ionic strength I of the solution. The program, based on the relationship between the interaction potentials and the structure factor, calculates a theoretical structure factor from three interaction potentials, *i.e.* a hard-core potential, a coulombic repulsion and a van der Waals attraction, which constitutes the DLVO model. These three potentials depend upon the sphere-equivalent diameter of the protein σ ($\sigma = 2R$). In addition, the repulsive coulombic potential is a function of the effective protein charge and of the ionic strength of the solution; the attractive van der Waals potential is characterized by its depth J (in k_BT units) and its range d (in Å) and depends upon the temperature. The theoretical structure factor determined by combination of these three potentials is then compared with the experimental one. The parameters (σ, Z, I, J and d) of the interaction potentials are modified until the experimental curves are correctly fitted on the whole s range.

If the only effect of pH and salt is to modify the net charge of the protein and the ionic strength of the solution, the two other parameters J and d remain constant, as the van der Waals potential is insensitive to variations in the concentration of electrolytes and pH. The diameter σ of urate oxidase is fixed at 70 Å from the crystallographic structure (Colloc'h *et al.*, 1997). With a tunnel whose volume represents only about 5% of the total volume, the enzyme can reasonably be considered to be a compact protein. The depth and the range of the van der Waals potential, expected to be constant for

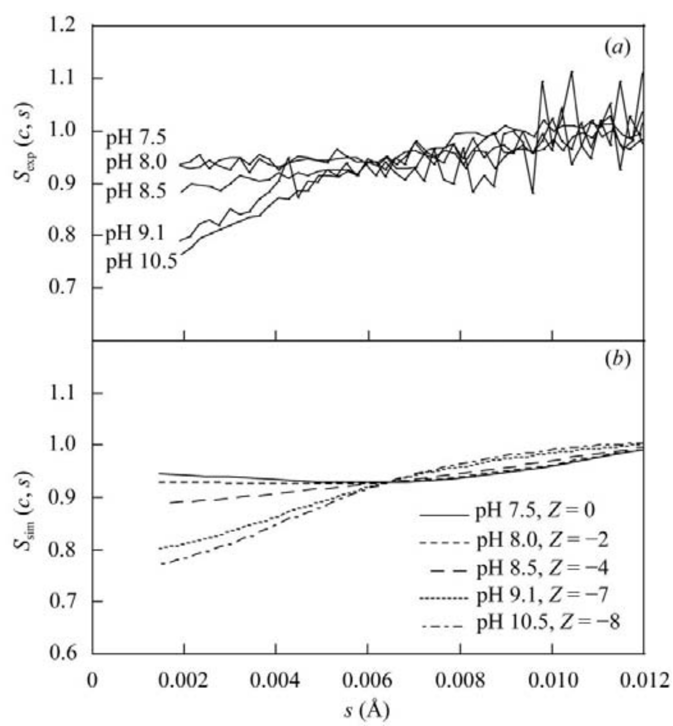

Figure 3
(*a*) Experimental structure factors of urate oxidase at 32 mg ml^{-1} as a function of pH; (*b*) corresponding simulated structure factors.

compact particles (Malfois *et al.*, 1996), were fixed to be about $2.5k_BT$ and 3 Å, respectively, at 293 K.

The experimental structure-factor curves at pH 7.5, 8.0, 8.5, 9.1 and 10.5 could be fitted using a calculated ionic strength of 0.025 *M* and a protein net charge of $Z = 0, -2, -4, -7$ and -8, respectively (Fig. 3), without changing any other parameters. The value of $Z = 0$ for pH 7.5 was expected as this is about the theoretical isoelectric point. In order to account for our experimental results at pH 8.5 and 10.5 with salt concentrations of 100 and 500 m*M* sodium acetate, respectively, we fitted the curves with respective ionic strengths of 0.125 and 0.525 *M* ([sodium acetate] + [buffer]), keeping the protein net charge (determined above at both pH) constant (not shown).

The theoretical study shows that considering the effect of salt only as a screening term, without specific consideration of anion or cation type, allows us to account for the experimental results.

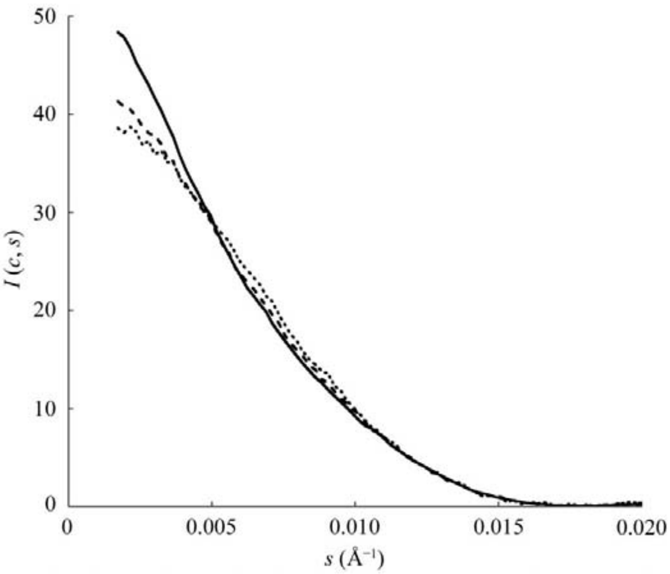

Figure 4
SAXS patterns of urate oxidase solutions in 50 m*M* Tris pH 8.5 at 293 K, with addition of 8% PEG 3350 at various concentrations of enzyme: 4 (dotted line), 16 (dashed line) and 32 mg ml^{-1} (continuous line).

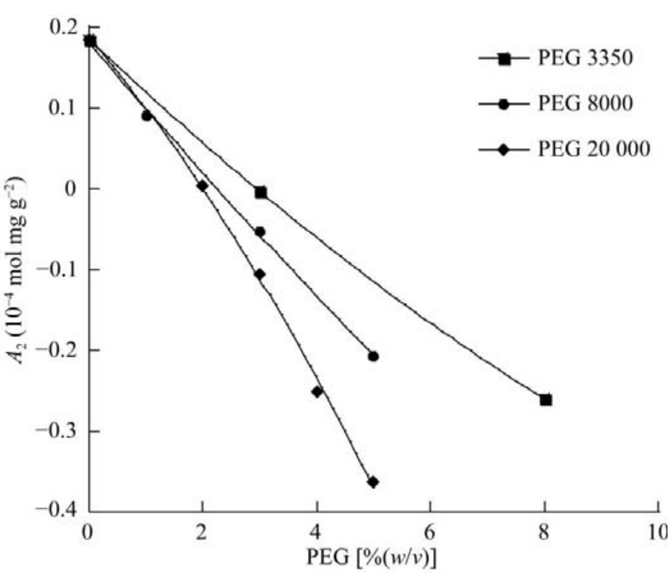

Figure 5
Second virial coefficient of urate oxidase as a function of percentage of different PEGs (the lines are drawn as guides).

4.4. PEG effects on interaction forces

In the previous study, PEG was shown to be efficient in inducing attractive interactions between molecules of urate oxidase at pH 9.1 in the presence of salt or at pH 8.5 without salt (Bonneté *et al.*, 2001). The PEG therefore seemed to be all the more effective when the coulombic repulsion was low, *i.e.* at a pH close to the pI or on screening the charges of the particle at pH values far from the pI.

In the present work, the effects of the concentration and the size of PEG were studied on urate oxidase interactions in solution. SAXS experiments were performed at pH 8.5 with three PEGs of different molecular weights: 3350, 8000 and 20 000 Da. The increase of the scattered intensity observed at small angles ($s < 0.005$ Å^{-1}) with the increase in protein concentration was indicative of attractive interactions between particles (Fig. 4). Expressed in terms of the second virial coefficient *via* (6), we observed that whatever the size of the polymer compared with the size of the protein, it was possible to reach an attractive regime corresponding to a negative second virial coefficient (Fig. 5) by increasing the polymer concentration. The efficiency of PEG in inducing more attractive interactions increases with the molecular weight and the concentration of the polymer. This result highlights the correlation between interactions in solution and solubility; Atha & Ingham (1981) showed that protein solubility decreases when the molecular weight and the concentration of the polymer increase.

4.5. Crystallization with PEG

In contrast to the case of salts, where no crystal was observed after several weeks at room temperature, crystals of urate oxidase grew in a few days from 30 mg ml^{-1} solutions of enzyme at pH 8.5 with different percentages of the three PEGs (Fig. 6).

As expected from a general protein concentration against % PEG diagram, for a given concentration of protein the nucleation rate increases with the PEG concentration and, in the same way, the PEG concentration necessary to crystallize the protein is lower when the size of PEG is larger. By correlating the different crystallization trials of urate oxidase in the three PEGs (3350, 8000 and 20 000) at pH 8.5 with the second virial coefficient in Fig. 5, we observed that the nucleation rate in the different crystallization drops follows the variation of A_2 and that the enzyme crystallizes in a very narrow range of A_2 values: $-0.40 < A_2 < 0.10$ ($\times 10^{-4}$ mol ml g^{-2}). The upper and lower limits of A_2 are those determined from growing crystals in the usual range of protein concentration (10–30 mg ml^{-1}). In this protein concentration range, higher concentrations of PEG led either to liquid–liquid phase separations, which can give crystals, or to amorphous precipitation.

In addition, different crystal habits were observed under the different PEG conditions used. These crystal shapes seemed to be more dependent upon the concentration of PEG and the supersaturation of the solution than upon the size of PEG. Whatever the molecular weight of PEG, for a low amount of PEG the crystals preferentially adopted a 'massive' polyhedral form, whereas for higher amounts of PEG they displayed a needle habit. Furthermore, the same shapes are observed for the conditions 5% PEG 3350, 4% PEG 8000 and 3 and 4% PEG 20 000 which correspond to an almost constant second virial coefficient. These results suggest that for a given initial protein concentration each crystal shape seems to correspond to a narrow range of the second virial coefficient (Fig. 6). Work is in progress to better characterize and understand the origin of these different crystal shapes.

5. Discussion

In the case of urate oxidase, monovalent or divalent salts only screen the protein charges through their ionic strength and do not induce attractive interactions and protein crystallization, in contrast to proteins such as lysozyme or BPTI. The failure of monovalent salts (at concentrations up to 1 *M*) to bring the overall interactions into an attractive regime have already been observed with other large proteins, *e.g.* aspartate transcarbamylase (ATCase; $R \simeq 60$ Å) from *E. coli* (Budayova *et al.*, 1999), α-crystallin ($R \simeq 85$ Å) from bovine lens (Finet, 1999; Finet & Tardieu, 2001) and with the brome mosaic virus (BMV; $R \simeq 135$ Å; Casselyn *et al.*, 2001). It may then follow that owing to this lack of attraction, monovalent salts alone are poorer crystallization agents for large particles than for small compact proteins. Even if in the case of urate oxidase sodium sulfate is inefficient to induce attractive interactions and crystallization, such a result cannot be extended to other large macromolecules since multivalent ions, whose effects are still poorly understood, are known to help in crystallizing or precipitating several large biological macromolecules (Ng *et al.*, 1996; Hempstead *et al.*, 1997).

For large macromolecules, PEG appears to be a far more efficient crystallization agent. Indeed, as for α-crystallin and ATCase, we observed that PEG induces attractive interactions between molecules of urate oxidase. We found that this attractive interaction increases with the concentration C_p and the size R_g of the polymer, R_g being evaluated by the expression R_g (Å) = $0.215\,M_w^{0.583}$, where M_w is the polymer molecular weight (Devanand & Selser, 1991). These variations of interactions were observed whatever the ratio of the R_g of the polymer to the radius R of the protein, *i.e.* $\xi = R_g/R$ ($\xi < 1$ for PEG 3350, $\xi \simeq 1$ for PEG 8000, $\xi > 1$ for PEG 20 000). Kulkarni *et al.* (2000) recently showed that the depletion attraction presents a minimum near the polymer concentration C_p^* [equal to $3M_w/(4\pi N_a R_g^3)$] at which polymers start overlapping (Kulkarni *et al.*, 2000). In our case, the second virial coefficient displays a monotonic decrease with the increase in PEG concentration even above C_p^* (for example, PEG 20 000 where $C_p^* \simeq 2.5\%$).

The addition of PEG induces the crystallization of urate oxidase, in a restricted second virial coefficient range −0.4 to +0.1 $\times$ 10^{-4} mol ml g^{-2}, at the low end of the 'crystallization slot' of George & Wilson (1994), which corresponds to the range −8 to −1 $\times$ 10^{-4} mol ml g^{-2}. Such behaviour has already been observed with other large proteins (Ebel *et al.*, 1999; Hitscherich *et al.*, 2000; Petsev *et al.*, 2001). All these results tend to confirm the theoretical work of Haas & Drenth (1998), which is based on the assumption that the first step of the protein crystallization mechanism, *i.e.* nucleation, occurs *via* a liquid–liquid phase separation. Indeed, for a small protein (MW = 14 kDa) they predicted an A_2 crystallization range of −3.5 to −9.0 $\times$ 10^{-4} mol ml g^{-2} and for a large protein (MW = 140 kDa), an A_2 crystallization range from −0.35 to −0.90 $\times$ 10^{-4} mol ml g^{-2} (assuming that both proteins have the same partial excluded volume equal to 0.74 cm^3 g^{-1}). Consequently, the second virial coefficient should be even further into the low-end part of the 'crystallization slot' of George & Wilson when the biological macromolecule is larger.

6. Conclusions

The results presented in this paper have shown that small-angle X-ray scattering can be a useful tool to characterize and understand protein interactions in solution and the mechanism of crystallization. The determination of the second virial coefficient A_2 from the SAXS measurements on dilute urate oxidase solutions appears in general to be a non-destructive method of predicting crystallization conditions. Studies of large macromolecules have confirmed that the addition of monovalent salts alone is often unable to induce attraction and to lead to crystallization. On the other hand, the study of urate oxidase (128 kDa) has underlined the important crystallizing power of a broad range of PEGs for large proteins.

We have shown that urate oxidase crystallizes in a restricted range of A_2 at the low end of the 'crystallization slot' described by George & Wilson for reasonable protein concentrations. It seems that this result can be generalized to all large proteins.

We also correlated variations of the second virial coefficient in various PEG with nucleation rates and crystals shapes.

Our studies emphasized the advantage of SAXS compared with the more common light scattering. Indeed, it is possible to obtain not only the zero-angle scattered intensity leading to A_2, but also the different underlying interaction potentials acting between the proteins in solution in various conditions by coupling SAXS experiments with numerical simulations in the whole s range. We have recently studied in the same way PEG–protein mixtures in crystallization conditions (Vivarès *et al.*, unpublished work). Work is in progress to characterize the influence of the protein size on the depletion attractive interaction induced by PEG addition. Such a study may enable us to obtain a general rule for protein crystallization with PEG.

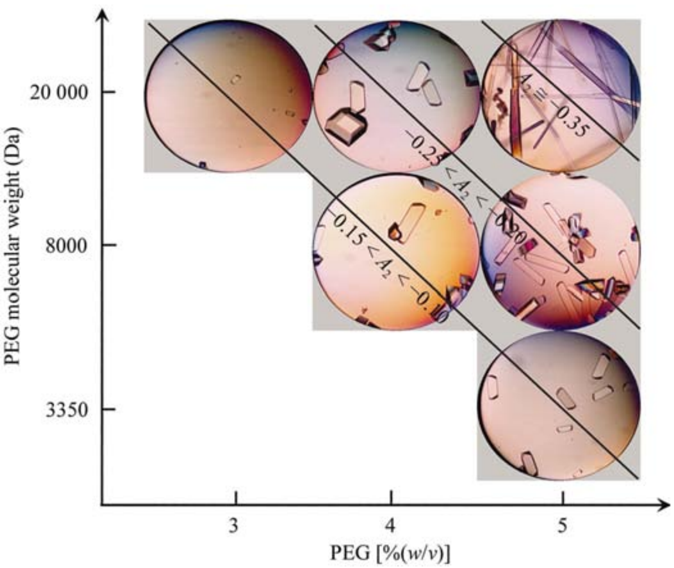

Figure 6
Crystals of urate oxidase (initial concentration 30 mg ml^{-1}) in 50 m*M* Tris pH 8.5 with various concentration of different PEGs. The diameter of each hole is 1300 µm. Each diagonal line corresponds to a narrow domain of A_2 (expressed in 10^{-4} mol ml g^{-2}) determined from Fig. 5.

We gratefully acknowledge M. El Hajji from Sanofi-Synthélabo (France) for generously providing us with urate oxidase and for his interest in this study. We thank A. Tardieu from LMCP-Paris and P. Vachette from LURE-Orsay for fruitful and critical discussions, and D. Myles from EMBL-Grenoble for re-reading the manuscript. We thank again P. Vachette and J. Perez from LURE-Orsay for their help during SAXS experiments on the instrument D24, and J. Perez for developing new programs for data treatment. The authors also gratefully acknowledge the financial support of CNES.

References

Asakura, S. & Oosawa, F. (1954). *J. Chem. Phys.* **22**, 1255–1256.
Atha, D. H. & Ingham, K. C. (1981). *J. Biol. Chem.* **256**, 12108–12117.
Bayol, A., Dupin, P., Boe, J. F., Claudy, P. & Létoffé, J. M. (1995). *Biophys. Chem.* **54**, 229–235.
Belloni, L. (1991). *Interacting Monodisperse and Polydisperse Spheres*, edited by P. Lindner & T. Zemb, pp. 135–155. North Holland: Elsevier.
Beynon, R. J. & Easterby, J. S. (1996). *Theory of Buffer Action.* Oxford: Blackwell Scientific.
Bonneté, F., Finet, S. & Tardieu, A. (1999). *J. Cryst. Growth*, **196**, 403–414.
Bonneté, F., Vivarès, D., Robert, C. & Colloc'h, N. (2001). *J. Cryst. Growth*, **232**, 330–339.
Boulin, C., Kempf, R., Koch, M. H. J. & McLaughlin, S. M. (1986). *Nucl. Instrum. Methods A*, **249**, 399–407.
Boyer, M., Roy, M. O., Jullien, M., Bonneté, F. & Tardieu, A. (1999). *J. Cryst. Growth*, **196**, 185–192.
Budayova, M., Bonneté, F., Tardieu, A. & Vachette, P. (1999). *J. Cryst. Growth*, **196**, 210–219.
Carbonnaux, C., Riès-Kautt, M. & Ducruix, A. (1995). *Protein Sci.* **4**, 2123–2128.
Casselyn, M., Perez, J., Tardieu, A., Vachette, P., Witz, J. & Delacroix, H. (2001). *Acta Cryst.* D**57**, 1799–1812.
Colloc'h, N., El Hajji, M., Bachet, B., L'Hermite, G., Schiltz, M., Prangé, T., Castro, B. & Mornon, J. P. (1997). *Nature Struct. Biol.* **4**, 947–952.
Depautex, C., Desvignes, C., Feder, P., Lemonnier, M., Bosshard, R., Leboucher, P., Dageaux, D., Benoit, J. P. & Vachette, P. (1987). *LURE: Rapport d'Activité pour la Période Août 1985–1987.* LURE, Orsay, France.
Derjaguin, B. V. & Landau, L. (1941). *Acta Physicochim. (USSR)*, **14**, 633.
Devanand, K. & Selser, J. C. (1991). *Macromolecules*, **24**, 5943–5947.
Dubuisson, J. M., Decamps, T. & Vachette, P. (1997). *J. Appl. Cryst.* **30**, 49–54.
Ducruix, A., Guilloteau, J. P., Riès-Kautt, M. & Tardieu, A. (1996). *J. Cryst. Growth*, **168**, 28–39.
Ebel, C., Faou, P. & Zaccai, G. (1999). *J. Cryst. Growth*, **196**, 395–402.
Finet, S. (1999). *Interactions entre Protéines en Solution: Étude par diffusion des Rayons X aux Petits Angles du Lysozyme et des Protéines du Cristallin; Application à la Cristallization.* Université Paris 6, Paris, France.
Finet, S. & Tardieu, A. (2001). *J. Cryst. Growth*, **232**, 40–49.
George, A. & Wilson, W. W. (1994). *Acta Cryst.* D**50**, 361–365.
Guo, B., Kao, S., McDonald, H., Asanov, A., Combs, L. L. & Wilson, W. W. (1999). *J. Cryst. Growth*, **196**, 424–433.
Haas, C. & Drenth, J. (1998). *J. Phys. Chem. B*, **102**, 4226–4232.
Haas, C., Drenth, J. & Wilson, W. W. (1999). *J. Phys. Chem. B*, **103**, 2808–2811.
Hempstead, P. D., Yewdall, S. J., Fernie, A. R., Lawson, D. M., Artymiuk, P. J., Rice, D. W., Ford, G. C. & Harrison, P. M. (1997). *J. Mol. Biol.* **268**, 424–448.
Hitscherich, C. J., Kaplan, J., Allaman, M., Wiencek, J. & Loll, P. J. (2000). *Protein Sci.* **9**, 1559–1566.
Hofmeister, F. (1888). *Arch. Exp. Pathol. Pharmakol.* **24**, 247–260.
Kulkarni, A. M., Chatterjee, A. P., Schweizer, K. S. & Zukoski, C. F. (2000). *J. Chem. Phys.* **113**, 9863–9873.
Lafont, S., Veesler, S., Astier, J. P. & Boistelle, R. (1997). *J. Cryst. Growth*, **173**, 132–140.
Lekkerkerker, H. N. W. (1997). *Physica A*, **244**, 227–237.
Mahadevan, H. & Hall, C. K. (1990). *AIChE J.* **36**, 1517–1528.
Malfois, M., Bonneté, F., Belloni, L. & Tardieu, A. (1996). *J. Chem. Phys.* **105**, 3290–3300.
Muschol, M. & Rosenberger, F. (1995). *J. Chem. Phys.* **103**, 10424–10432.
Ng, J. D., Lorber, B., Witz, J., Théobald-Dietrich, A., Kern, D. & Giegé, R. (1996). *J. Cryst. Growth*, **168**, 50–62.
Petsev, D. N., Thomas, B. R., Yau, S. T., Tsekova, D., Nanev, C., Wilson, W. W. & Vekilov, P. G. (2001). *J. Cryst. Growth*, **232**, 21–29.
Petsev, D. N., Thomas, B. R., Yau, S.-T. & Vekilov, P. G. (2000). *Biophys. J.* **78**, 2060–2069.
Petsev, D. N. & Vekilov, P. G. (2000). *Phys. Rev. Lett.* **84**, 1339–1342.
Piazza, R. & Pierno, M. (2000). *J. Phys. Condens. Matter*, **12**, A443–A449.
Riès-Kautt, M. & Ducruix, A. (1989). *J. Biol. Chem.* **264**, 745–748.
Tardieu, A., Le Verge, A., Riès-Kautt, M., Malfois, M., Bonneté, F., Finet, S. & Belloni, L. (1999). *J. Cryst. Growth*, **196**, 193–203.
Veesler, S., Lafont, S., Marcq, S., Astier, J. P. & Boistelle, R. (1996). *J. Cryst. Growth*, **168**, 124–129.
Velev, O. D., Kaler, E. W. & Lenhoff, A. M. (1998). *Biophys. J.* **75**, 2682–2697.
Verwey, E. J. W. & Overbeek, J. T. G. (1948). *Theory of the Stability of Lyophobic Colloïds.* Amsterdam: Dover.
Vliegenthart, G. A. & Lekkerkerker, H. N. W. (2000). *J. Chem. Phys.* **112**, 5364–5369.
Vrij, A. (1976). *Pure Appl. Chem.* **48**, 471.